Integrated Power Simulation for a Solar-Powered, Computationally-Intensive Unmanned Aircraft

Or D. Dantsker*, Mirco Theile†, and Marco Caccamo ‡
Technical University of Munich, Garching, Germany

Seongyong Hong§
University of Illinois at Urbana–Champaign, Urbana, IL 61801

In recent years, we have seen an uptrend in the popularity of UAVs driven by the desire to apply these aircraft to areas such as precision farming, infrastructure and environment monitoring, surveillance, surveying and mapping, search and rescue missions, weather forecasting, and more. A major technical hurdle to overcome is drastically reducing the overall power consumption of these UAVs so they can be powered by solar arrays and for long periods of time. This paper presents simulation results for a long-endurance, solar-powered unmanned aircraft, using an integrated aircraft power model for solar generation and aircraft propulsion. These power consumption and generation models are described, derived, and integrated into a cohesive system-wide aircraft power model, presented in the form of a systemic flow diagram. Power balance expressions are also imposed based on temporal and physical constraints. The UIUC-TUM Solar Flyer, a computationally-intensive, long-endurance solar-powered unmanned aircraft, is an example aircraft for the simulation. Trajectory and time parameters from a recent long-endurance flight are used to define the simulation conditions. The results of the simulation are then compared to the experimental flight test results.

Nomenclature

ESC	=	electronic speed controller	$E_{battery,max}$	=	battery energy capacity
GaAs	=	gallium arsenide	$\vec{F}$	=	force vector
MPPT	=	maximum power point tracker	g	=	gravitational acceleration
NREL	=	National Renewable Energy Laboratory	i_m	=	motor current
RPM	=	rotations per minute	i_0	=	zero load motor current
SPA	=	Solar Position Algorithm	I_{solar}	=	solar flux
UAV	=	unmanned aerial vehicle	J	=	advance ratio
			K	=	aerodynamic constant
$\vec{a}$	=	aircraft acceleration vector	K_i, K_p	=	propulsion model constants
A_{array}	=	solar array area	K_v	=	motor speed constant
C_D	=	drag coefficient	L	=	lift force
C_{D_o}	=	parasitic drag coefficient	L/D	=	lift-to-drag ratio
C_L	=	lift coefficient	m	=	aircraft mass
C_P	=	power coefficient	n	=	propeller and motor rotation rate
C_T	=	thrust coefficient	P	=	power
D	=	propeller diameter, drag	$P_{avionics}$	=	avionics power consumption
$E_{battery}$	=	battery energy	$P_{battery}$	=	battery power (output positive)

*Researcher, Department of Mechanical Engineering, or.dantsker@tum.de
†Ph.D. Student, Department of Mechanical Engineering. mirco.theile@tum.de
‡Professor, Department of Mechanical Engineering, mcaccamo@tum.de
§Undergraduate Student, Department of Aerospace Engineering, sh36@illinois.edu.

$P_{computation}$	=	computation power consumption	$\hat{u}_{array}$	=	solar array unit direction
P_{dyn}	=	dynamic power	$\hat{u}_{sun}$	=	sun ray unit direction
P_{ESC}	=	ESC output power	U_m	=	motor terminal voltage
P_{FM}	=	flight mechanics power	v	=	velocity
P_{in}	=	input power to power bus	$\vec{v}$	=	velocity vector
P_{motor}	=	motor output power	w	=	solar array normal direction
P_{other}	=	other device power consumption	W	=	weight
P_{out}	=	output power from power bus			
$P_{propulsion}$	=	propulsion power consumption	$\chi(P_{battery})$	=	battery efficiency (piece-wise)
P_{sensor}	=	sensor power consumption	γ	=	climb angle
P_{shaft}	=	shaft output power	η_{array}	=	solar array angular efficiency
$P_{soaring}$	=	soaring power generation	$\eta_{battery,in}$	=	battery charging efficiency
P_{solar}	=	solar array power generation	$\eta_{battery,out}$	=	battery discharing efficiency
P_{ss}	=	steady state power	η_{ESC}	=	ESC efficiency
P_{thrust}	=	aerodynamic thrust power from propeller	η_{motor}	=	motor efficiency
q	=	dynamic pressure	η_{MPPT}	=	MPPT efficiency
Q	=	torque	$\eta_{propeller}$	=	propeller efficiency
R_m	=	internal motor resistance	η_{solar}	=	solar array/cell conversion efficiency
S	=	wing area	ϕ	=	roll (bank) angle
t	=	time	ρ	=	density of air
t_o	=	initial time	$\theta_{sun-array}$	=	relative sun-array angle
T	=	thrust, current time			
T_{ss}	=	steady state thrust			

I. Introduction

In recent years, we have seen an uptrend in the popularity of UAVs driven by the desire to apply these aircraft to areas such as precision farming, infrastructure and environment monitoring, surveillance, surveying and mapping, search and rescue missions, weather forecasting, and more. The traditional approach for small size UAVs is to capture data on the aircraft, stream it to the ground through a high power data-link, process it remotely (potentially off-line), perform analysis, and then relay commands back to the aircraft as needed.[1–5] Given the finite energy resources found onboard an aircraft (battery or fuel), traditional designs significantly limit aircraft endurance since significant power is required for propulsion, actuation, and the continuous transmission of visual data. All the mentioned application scenarios would benefit by carrying a high-performance embedded computer system to minimize the need for data transmission. A major technical hurdle to overcome is that of drastically reducing the overall power consumption of these UAVs so that they can be powered by solar arrays. The process of reducing aircraft power consumption is required to reduce aircraft weight, prolong flight time, and ultimately reduce the cost to support the widespread adoption of UAVs for different types of missions. To do so, the power requirement of an aircraft and the conversion efficiencies of its various systems must be modeled and parametrized. Only then system-wide simulation and optimization can be performed.

Currently, the UIUC-TUM Solar Flyer[6] is being developed and flight-tested to enable a variety of all-daylight missions to be performed, involving the continuous acquisition and processing of high resolution visible and infrared imagery. A key resource in aircraft development has been the formulation of a holistic, integrated power model that can encompass power generation and consumption such that further aircraft and mission design, simulation, and optimization can be performed. Previous works have separately looked at electric aircraft modeling,[7–10] solar aircraft modeling,[11–15] and propulsion system modeling[16–23] with varying degrees of assumptions. Similarly, others have also looked into aircraft dynamics modeling for the purpose of creating accurate simulation.[24–27] Compared to works in

the existing literature, the model developed, which is briefly described below, follows a holistic approach for UAV modeling that encompasses aircraft, propulsion, and solar models under realistic assumptions.[28]

The paper is organized as follows. First, an abridged derivation of the integrated power model for solar-powered, computationally-intensive unmanned aircraft is given, including the temporal and physical power balance expressions and the power models for solar generation and aircraft propulsion. This is followed by an overview of the UIUC-TUM Solar Flyer and a presentation of flight data from a 1 hour flight performed under ideal conditions. The integrated power simulation is then described, including its implementation and the parameters used. Next, a simulation attempting to duplicate the aforementioned 1 hour flight is presented. The simulated results are then described and compared to the experimental flight performed. The paper concludes with a summary and statement of future work.

II. Integrated Power Model

An integrated power model was developed for a long-endurance, solar-power type aircraft, such as the UIUC-TUM Solar Flyer. The integrated model, which is visualized in Figure 1, provides a complete system-level mathematical description from which future power-aware aircraft design, integration, and optimization can be made. The core elements of this model are power generation, power consumption, power distribution, and energy storage.

Power generation elements modeled in the integrated aircraft power model include a solar position and radiation model, a solar array model, and a maximum power point tracker (MPPT) solar charge controller model. The integrated aircraft power model also enables integration of soaring harvested from thermal updrafts and wind shear, i.e., thermal and dynamic soaring. However, specific modeling techniques for power collection through soaring will not be included in the scope of the current work – many can be found in existing literature.[29–34]

In terms of power consumption, elements are categorized into propulsion, avionics, and others. Propulsion power is computed using a flight mechanics model, thrust model, motor model, and an electronic speed controller (ESC) model. The avionics power is computed from the baseline and flight conditions of the avionics components, which include the flight control and data acquisition system, the computational platform, and the sensors. Other power-consuming elements include such components as actuators and navigation lights.

Power distribution onboard the aircraft is handled by a power bus, which for the purpose of this work is assumed to be transparent, i.e., no losses are incurred in transmission through the power bus. Finally, energy storage is stored in two forms: electrical/chemical energy in the form of batteries and mechanical energy in the form of aircraft potential and kinetic energy.

A. Power Balance

In order to enable long-endurance flight, the temporal power balance is maintained. Specifically, that the amount of power that is being consumed over time is less than that available from solar power collection sources and the battery. Thus, at the power distribution bus in Figure 1, it must always hold that,

$$0 = P_{out}(t) - P_{battery}(t) - P_{in}(t), \quad \forall t \in [t_0, T] \tag{1}$$

with t_0 being the time of take-off and T being the time of landing. Note that positive battery power $P_{battery}$ signifies the outward flow of power from the battery, i.e., the battery is being discharged. Conversely, negative battery power signifies power flowing into the battery, i.e., the battery is being charged.

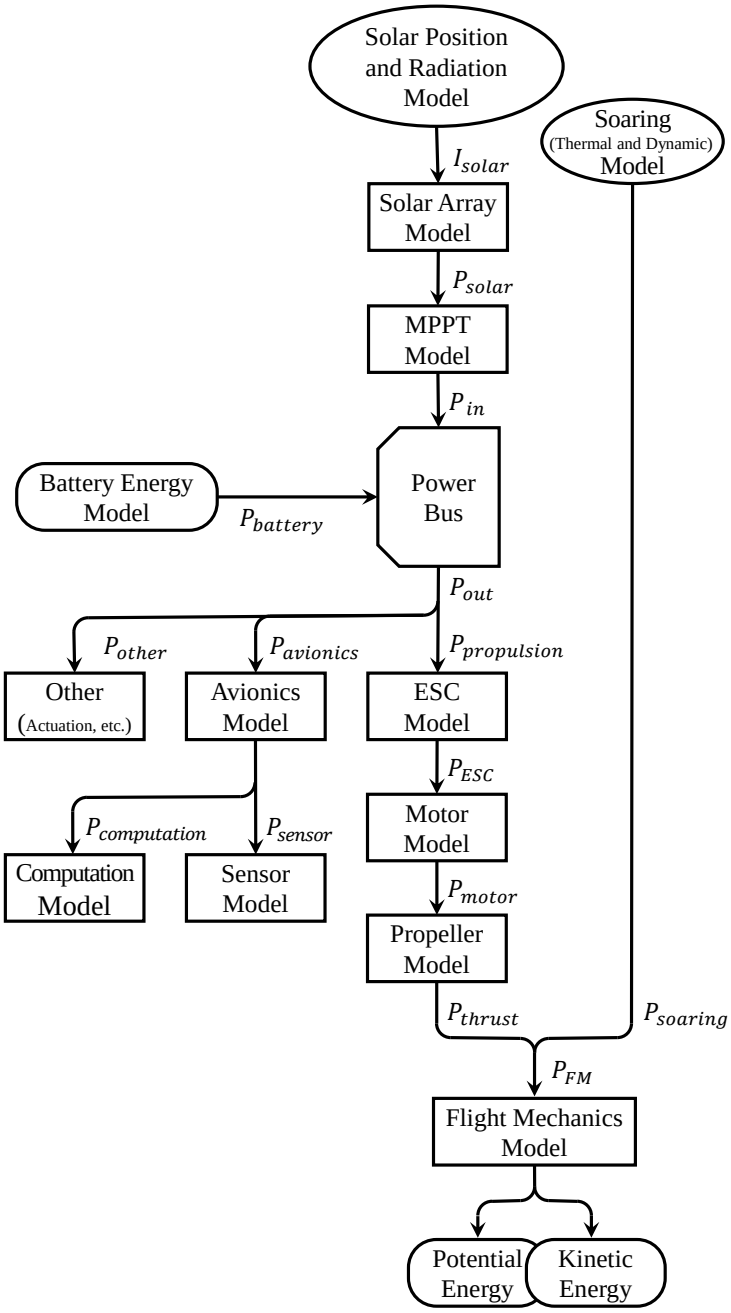

Figure 1: Diagram of the integrated power model for a long-endurance, solar-power type aircraft.

Additionally, it must be imposed that the battery may only hold energy equivalent to less than or equal to its energy capacity,

$$0 \leq \int_{t_0}^{t} \chi(P_{battery}) \cdot P_{battery}(s)ds + E_{battery}(t_0) \leq E_{battery,max}, \quad \forall t \in [t_0, T] \tag{2}$$

in which

$$\chi(P_{battery}) = \begin{cases} \eta_{battery,in} & \text{if } P_{battery} < 0 \\ \frac{1}{\eta_{battery,out}} & \text{if } P_{battery} \geq 0 \end{cases} \tag{3}$$

The above equation effectively defines the limitation of the battery's ability to retain and store energy within its capacity limits and takes into account efficiency losses of charging ($\eta_{battery,in}$) and discharging ($\eta_{battery,out}$) the battery. Since $P_{battery}$ is measured at the bus, $\frac{1}{\eta_{battery,out}} \cdot P_{battery}$ is drawn from the battery when discharging. It should be noted that for the cases where the battery is fully charged, and excess power is being generated and not used, i.e., $P_{out} < P_{in}$, the excess power will not be rejected in the form of heat being shed from the solar arrays.

B. Solar Power Generation

In order to maintain a sufficient energy buffer, it is essential to balance energy consumption with energy generation. Therefore, developing a high-fidelity model for solar power generation is vital for the continued operation of a long-endurance, solar-powered unmanned aircraft. Solar-power generation will vary based on physical phenomena, i.e., solar position and radiation, and the performance of aircraft hardware components, i.e., the solar array and MPPT charge controller. Models for solar position and radiation and the solar array are described below. For the scope of this work, MPPT charge controllers are simply assumed to have fixed efficiency loss, as commonly described in the literature.[13,19,23,35]

The solar potential of an energy harvesting component depends on two external factors: the sun's position, thereby yielding the direction of the sun rays, and the radiation, thereby yielding flux that can be harvested. These factors have been studied for many years and are well parameterized and modeled.[36–40] A standard source for determining the position of the sun is the U.S. Department of Energy, National Renewable Energy Laboratory (NREL) Solar Position Algorithm (SPA).[41] The relative position of the sun is then used to calculate the incidence between the solar array direction and the sun rays.

There are many ways to estimate solar radiation, i.e., solar flux, available for harvesting. Similar to the position of the sun, the quantity of available solar flux depends on date, time, and location. However, the quantity of solar flux also depends on atmospheric conditions such as cloud amount and layering, precipitation, fog/smoke, etc.[42] Many sources outline different methods to estimate solar flux as well as provide libraries to calculate solar flux.[43,44] Many works in the literature also estimate solar flux using random distributions.[34]

Solar arrays' energy production relies on the ability to convert solar radiation into electrical energy. The effectiveness of this energy conversion process depends on two factors: conversion efficiency and off-angle performance. These factors are analogous and depend on the factors affecting solar potential. The first major factor that affects the performance of solar arrays is the conversion efficiency of the cells. This efficiency is dependent on the chemistry and design of the photo-voltaic cells being used. Specifically, solar cell efficiency factors are reflectance, thermodynamic efficiency, charge carrier separation efficiency, charge carrier collection efficiency, and conduction efficiency values. The efficiency of a given photo-voltaic cell is affected by external factors such as ambient temperature, spectrum, and flux. Therefore, cell efficiency is often modeled as either a variable of the factors above or a single value based on the dominant conditions. The second major factor that affects the performance of solar arrays is off-angle performance. More often than not, solar arrays are not oriented orthogonally to the direction of the sun rays and thus only receive solar radiation equivalent to the flux multiplied by the projected area. However, as solar cells do not have ideal off-angle performance, the above expression must be re-written with a function of relative angles between the array direction and the sun rays, $\eta_{array}(\theta_{sun-array})$.

However, determining the relative orientation of the aircraft solar arrays with respect to the solar rays is complicated. The aircraft is continually moving and often reorienting, and the solar arrays are hardly oriented in a single flat plane. Specifically, these complications depend on the aircraft's geometry, orientation, and wing flex. An example aircraft geometry with the solar array normal vectors being offset from the aircraft reference normal is visualized in Figure 2 for the UIUC-TUM Solar Flyer; knowledge of such geometry allows the baseline angular offset to be calculated.

Meanwhile, to determine aircraft orientation, the aircraft trajectory is used to directly output bank, i.e., roll angle and climb angle. Using the trajectory, the expected load factor can be estimated based on the curvature, which knowing the aircraft's lift curve slope, allows angle-of-attack to be computed. The aircraft pitch angle can then be determined from the angle-of-attack and climb angle. Similarly, wing flex will be estimated based on aircraft loading, which can be ascertained from the aircraft trajectory state. The advantage of this method is that neither angle-of-attack nor aircraft loading need to be directly measured.

Therefore, as derived in previous work,[28] an aircraft with n solar arrays with identical conversion and angular performance will generate solar power following:

$$P_{solar} = I_{solar}\eta_{solar}\sum_{i=1}^{n} A_{array_i}\eta_{array}(\arccos(\hat{\mathbf{u}}_{\mathbf{sun}} \cdot \hat{\mathbf{u}}_{\mathbf{array_i}})) \tag{4}$$

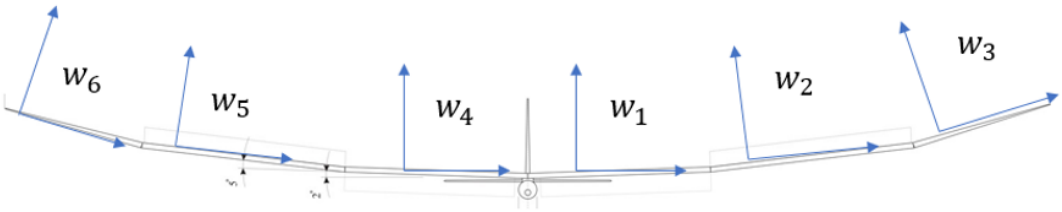

Figure 2: Solar array orientations of the UIUC-TUM Solar Flyer.

C. Aircraft Propulsion Power Consumption

On an electric UAV, there are a series of propulsion system power-consuming components. The below propulsion power model analytically explains how power flows from the energy source into thrust power. First, the energy source, e.g., battery or solar collection system, provide the propulsion power; electronic speed controller (ESC) routes the electric power via the wire leads to the motor poles in order to induce rotation with an efficiency loss; then, the motor converts the electric power into rotational power to drive the propeller, also with an efficiency loss; after that, the propeller converts the rotation power into thrust power, applying a forward thrust force to the aircraft - with an efficiency loss. Thus, the product of the propulsion power, ESC efficiency, motor efficiency, and propeller efficiency is the thrust power:

$$P_{propulsion} \cdot \eta_{ESC} \cdot \eta_{motor} \cdot \eta_{propeller} = P_{thrust} \tag{5}$$

In order to make the power consumption model as versatile as possible, state variable inputs are restricted to easily measurable values. Specifically, the variable inputs are properties of the aircraft maneuver, including velocity, acceleration, roll (bank) angle, and climb angle. Doing so requires certain assumptions[a], which will work well for the overwhelming majority of long-endurance UAV flights. Therefore, the power model provides an estimation based on the motion of the aircraft, i.e., flight path, with minimal knowledge of the aircraft flight mechanics attributes. Figure 3 shows how the model is cascaded from the input variables through a flight mechanics model, a propeller model, a motor model, and an ESC model. This follows the high-level explanation mentioned above, similar to Figure 1, but in a backward manner. It should be noted that for the purpose of the propulsion power derivation, thrust power P_{thrust} will be set equal to flight mechanics power P_{FM}, i.e., soaring power $P_{soaring}$ will temporarily be set to zero, as adjustments can easily be implemented by decreasing thrust power in Equation (5).

[a]It is assumed that angle-of-attack is relatively constant, incidence angle is approximately zero, and thus climb angle is approximated as the measurable pitch angle. Additionally, it is assumed there is minimal side-slip allowing for turn radius to be calculated directly from the roll angle.

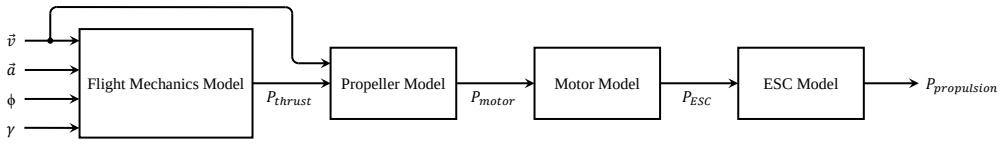

Figure 3: Aircraft propulsion power modeling based on aircraft state.

The flight mechanics model takes into account power required for steady-state flight as well as dynamic maneuvers. Specifically, the total thrust power is given by

$$P_{thrust} = P_{ss} + P_{dyn} \tag{6}$$

The steady-state power portion of the thrust power, P_{ss}, is calculated from steady-state maneuver data that can be measured or simulated, including velocity v, roll (bank) angle ϕ, and climb angle γ. Figure 4 shows these state variables applied to level, turning, and climbing flight [b]. The remainder of the steady-state portion of the propulsion power model will be derived from elementary flight mechanics principles.[45] Assumptions of constant lift-to-drag ratio and of non-constant lift-to-drag ratio were made in a previous derivation set;[46] however, for the sake of brevity and accuracy, only the non-constant lift-to-drag ratio assumption derivation is presented.

$$P_{ss} = \frac{1}{2}\rho S C_{D_o} v^3 + \frac{2Km^2g^2}{\rho S}\frac{\cos^2\gamma}{v\cos^2\phi} + mgv\sin\gamma \tag{7}$$

This expression can be simplified by assigning constants

$$P_{ss} = K_p v^3 + K_i \frac{\cos^2\gamma}{v\cos^2\phi} + mgv\sin\gamma \tag{8}$$

where

$$K_p = \frac{1}{2}\rho S C_{D_o} \tag{9}$$

$$K_i = \frac{2Km^2g^2}{\rho S} \tag{10}$$

It should be noted that these constants can be calculated from aircraft data; however, without pre-existing aircraft performance data, the constants are more easily determined from training data using linear regression with a non-linear kernel.

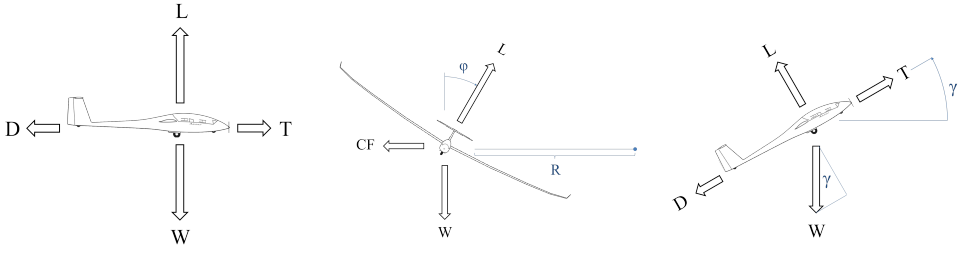

(a) (b) (c)

Figure 4: Steady-state forces on an aircraft in (a) level flight, (b) turning flight and (c) climbing flight.

The steady-state power is only valid for steady-state maneuvers and greatly differs from total thrust power in maneuvers incorporating acceleration. However, it is still useful in calculating the total thrust power in such maneuvers. To incorporate the dynamics into the power model, dynamics power, P_{dyn}, is added. The dynamic power is calculated based on Newton's second law as

$$P_{dyn}(\vec{a},\vec{v}) = m(\vec{a}\cdot\vec{v}) \tag{11}$$

[b] Note that based on the above-stated assumptions, velocity is in the thrust direction.

It is assumed that the effect of rotational accelerations is negligible. Additionally, the model can be extended to take into account constant wind as well as wind gusts by modifying $\vec{v}$ and $\vec{a}$ in the previous expressions.

With the calculated thrust power, the ESC, motor, and propeller efficiencies can now be incorporated to calculate the input power needed to produce this thrust. The relation is given by rearranging Equation (5)

$$P_{propulsion} = \frac{P_{thrust}}{\eta_{ESC} \cdot \eta_{motor} \cdot \eta_{propeller}} \tag{12}$$

The efficiency factors themselves depend on numerous factors that are directly or indirectly related to thrust and velocity and aircraft power system configuration, e.g., battery voltage. There have been a variety of derivations developed for computing ESC efficiency.[7,16,17] These generally yield that ESC efficiency is a function of voltage and current. The duty cycle, which is proportional to shaft rotation rate or throttle input, is often also considered. For the scope of the current work, ESC efficiency will be fixed to a constant value, which is representative of its efficiency at cruise conditions, i.e., ESC efficiency curves have been shown to flatten out once reaching a small percentage of their design operating current.[17]

Propeller efficiency can be derived using blade element momentum theory (BEMT) and sectional airfoil theory as done in.[47] However, BEMT curves are highly sensitive to variations of the parameters used. In order to increase model accuracy, experimental data for propeller performance can be obtained from wind tunnel propeller testing[22,48] and an existing database,[49,50] with interpolation being done as required. The process of determining the propeller efficiency for each given flight state follows the method presented in previous work.[51]

Methods exist to determine motor efficiency. For example, a first order approximation by Drela[52] estimates motor efficiency as a function of motor voltage and rotation rate and the three aforementioned motor parameters.

$$\eta_{motor}(n, U_m) = \left(1 - \frac{i_0 R_m}{U_m - 60n/K_v}\right) \frac{60n}{U_m K_v} \tag{13}$$

A second order approximation[53] also exists. However, it requires a fourth motor parameter, K_Q, the motor torque constant, which is not easily obtained from manufacturers but instead needs to be measured through dynamometer benchtop testing.[16]

Combining the steady-state and dynamic thrust power models and the propeller and motor models yields

$$P_{propulsion}(\vec{v}, \vec{a}, \phi, \gamma) = \frac{K_p v^3 + K_i \frac{\cos^2\gamma}{v\cos^2\phi} + mgv\sin\gamma + m\vec{a}\cdot\vec{v}}{\eta_{propeller} \cdot \eta_{motor} \cdot \eta_{ESC}} \tag{14}$$

where K_p, K_i, and η_{ESC} were defined earlier and $\eta_{propeller}$ and η_{motor} are determined iteratively for each state using the *Rotation Rate and Efficiency Algorithm* and *Propeller Rotation Rate Subroutine* techniques presented in previous work.[51]

The aircraft propulsion power model was evaluated through flight testing using an existing, instrumented aircraft, which had been used extensively for avionics development and other purposes. The aircraft was autonomously flown through a reference flight path, which contained turns, climbs, descents, and straight-line segments. The flight testing showed very close agreement between the power and energy estimates determined using the power model from aircraft state data and actual experimental power and energy measurements, within less than 5%.[46,51]

III. Solar-Powered Aircraft

A. Aircraft Overview

The UIUC-TUM Solar Flyer is a computationally-intensive, long-endurance solar-powered unmanned aircraft, which is shown in Fig. 5. In order to keep the aircraft relatively inexpensive, both in labor and cost, the aircraft has been developed using a majority of commercial-off-the-shelf components, which highly limits the number of viable options. The airframe chosen for development was selected through trade studies [54] that considered airframe availability and payload requirements as well as potential energy collection – more detail regarding airframe selection and integration can be found in related literature.[6,54,55] In similar recent related work, a propulsion system optimization tool was developed and validated[51] and then applied to the UIUC-TUM Solar Flyer.[56]

The 4.0 m (157 in) wingspan UIUC-TUM Solar Flyer aircraft weighs approximately 3.3 kg (7.2 lb). It is powered by a 64 W gallium arsenide (GaAs) solar array used in conjunction with a maximum power point tracking (MPPT) charge controller and a 3S 8P, 10.8V 28Ah 18650 lithium-ion battery that acts as an energy buffer. The UIUC-TUM Solar Flyer avionics are based around a commercially available flight control and data acquisition system, the Al Volo FC+DAQ,[57,58] and uses the open-source uavAP autopilot[59,60] and uavGS ground station interface.[61,62] The system integrates a 9-DOF inertial measurement unit (IMU) and 10 Hz Global Navigation Satellite System (GNSS) and operates at 100 Hz. The aircraft is instrumented with an airspeed probe and sensor as well as various power sensors distributed throughout the aircraft. Data is downlinked in-flight using a 900 MHz radio module. Further detail regarding the UIUC-TUM Solar Flyer specifications can be found in related literature.[63]

Figure 5: The UIUC-TUM Solar Flyer aircraft.

B. Reference Flight Testing Results

During the 2020 flight season, the UIUC-TUM Solar Flyer performed several long-endurance, solar-powered flights. Of them, the longest flight performed was an 8-hour flight in August 2020 under non-ideal (cloudy and windy) weather conditions.[64] For this paper and providing a benchmark for simulation, a 1-hour flight performed under ideal conditions is presented as a point of reference.

An approximately 1-hour flight was performed on Oct 8, 2020, under ideal conditions. The UIUC-TUM Solar Flyer took off at 11:43 AM and landed at 12:40 PM local time. The sun shifted from 42 deg elevation and 158 deg azimuth to 45 deg elevation and 177 deg azimuth during that time. A nearby national weather station reported that winds were calm to 3 mph (1.3 m/s) from a variable direction and that it was sunny with fair skies (less than 40% clouds). Locally at the field, the flight crew observed sunny skies with winds of 3-5 mph (1.3-2.2 m/s) from the SSW (190-210 deg), which was aligned with the runway, from right to left (in the perspective of the flight crew).

The trajectory of the flight is shown in Fig. 6. The figure is laid out from above the flight crew area, looking towards the flight testing area and the aircraft flight path. The takeoff was performed from the runway using a dolly, from left to right, followed by an ascent into a clockwise race track flight pattern. Specifically, the aircraft was commanded to perform a race track pattern of 650×150 m at an altitude of 100 m AGL; and maintain an airspeed of 11 m/s. The aircraft performed 26 laps of the flight pattern with some deviations that are addressed below. This was followed by a descent to landing. The landing was performed from left to right on a grass strip parallel to the runway.

The race track path flown is equivalent to an area coverage mission with 500 m long straights that are 150 m apart, with required 180 deg, 75 m radius turn-arounds at the ends of the straights. As mentioned, 26 laps were performed during the 53 min of maneuvering, yielding an effective coverage area of 1.95 km^2 (481 acres). Therefore, the race track maneuvering demonstrated equates to an area coverage of 2.2 km^2/hr (545 $acre/hr$).

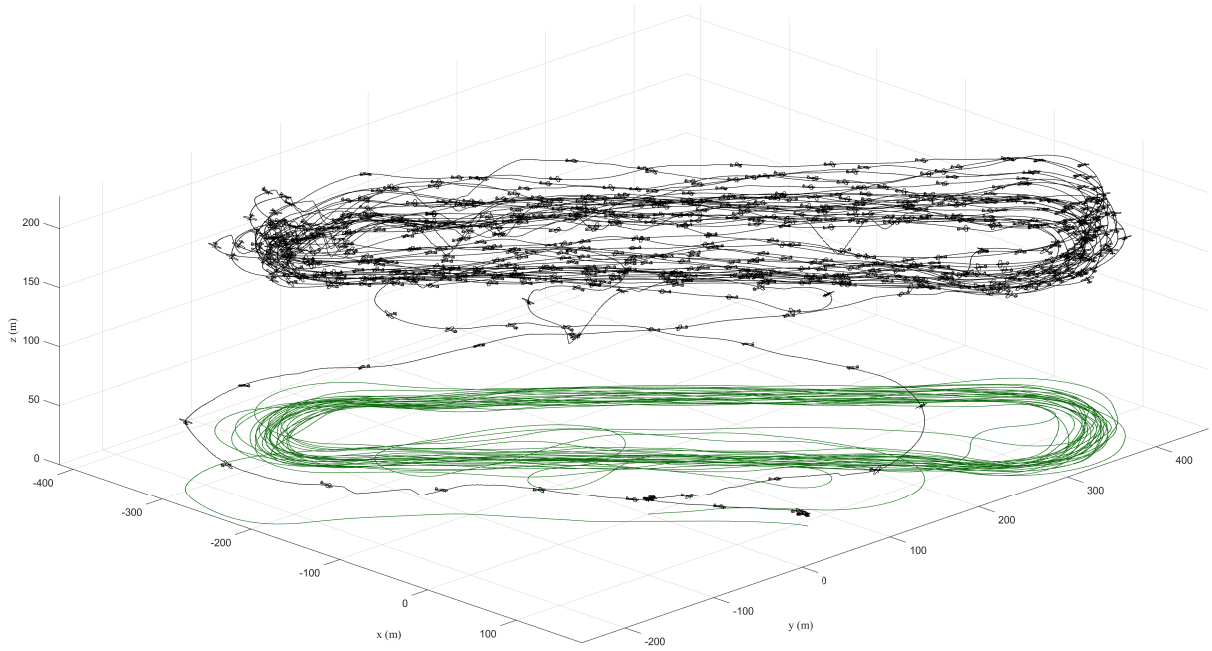

Figure 6: The trajectory of the UIUC-TUM Solar Flyer performing the approximately 1 hour flight under ideal conditions (note that the aircraft is plotted every 5 sec).

The state data time history is presented in Fig. 7. The aircraft position, Northing and Easting, and the altitude are presented in (a) and (b), respectively; note that the runway altitude is lower than the ground level of the maneuvering area due to the flight site geography yielding an altitude difference of greater than 100 m. The Euler angle pitch and roll are presented in (c), and heading is presented in (d). The aircraft air and ground speeds are presented in (e); the ground speed is measured by the GNSS, while the airspeed is computed by a wind-tunnel calibrated pitot-probe airspeed sensor. The propulsion power, measured at/between the battery and ESC, is presented in (f). The propeller rotation rate, measured by the ESC, is presented in RPM in (g). The battery voltage is presented in (h), and the solar power generated by the solar arrays is presented in (i).

The position and Euler angle data show 26 race track laps being performed, each approximately 2 min long. There are an increasing amount of primarily positive vertical excursions from the commanded altitude during the middle part of the flight. The airspeed data shows an attempt to maintain the 11 m/s commanded airspeed with increased airspeeds correlating to when the positive vertical excursions occurred. There are also repeated offsets between air and ground speed, which result from wind; the magnitude is either positive or negative based on whether the aircraft is flying upwind or downwind.

The aircraft propulsion power heavily oscillates during the entire flight from 0 to 230 W. There is a decrease in the on-power times used during the middle of the flight when positive vertical excursions occurred; these are also the same times when the airspeed exceeded the commanded 11 m/s. It is assumed that the uncommanded positive altitude deviations are the result of thermals. During this time, the ESC throttles the motor off with the propeller windmilling. Meanwhile, the negative altitude deviations seem to result from an interplay between the autopilot attempting to pitch the aircraft down to maintain altitude and, often, the thermals weakening. As a result, the ESC is commanded to throttle up the motor to create thrust and increase airspeed, corresponding to propulsion power consumption.

Thus, the throttling-on and throttling-off of the motor result from the interplay between the autopilot and ESC controllers and limits. With the earlier thermal assumption, it is assumed that some of the energy used to propel the aircraft and counter drag also comes from thermals through the uncommanded altitude and thus potential energy gains. In order to better estimate propulsion power consumption, 10 min moving averages of the race track laps were calculated, comprising five laps of 60,000 data points each, yielding average power values between 14 and 53 W. Due to the large difference in 10 min average values, an actual average propulsion power consumption value could not definitively be calculated. As expected, the propeller rotation rate correlates with the propulsion power, i.e., when propulsion power is high, the propeller rotation rate increases to approximately 6,400 RPM, while when propulsion power is near 0, the propeller rotation rate decreases to approximately 2,900 RPM. This indicates the ESC throttling the motor on when the airspeed dips below 11 m/s and then off when it is above that airspeed.

Except for an oscillation during takeoff, the battery voltage remains constant at 12.05 V for the entire flight. Finally, the solar power is observed to vary cyclically between 14 and 55 W, correlating to the repeated re-orientation of the aircraft as laps are being performed. Over the entire flight, the average solar power was approximately 35 W.

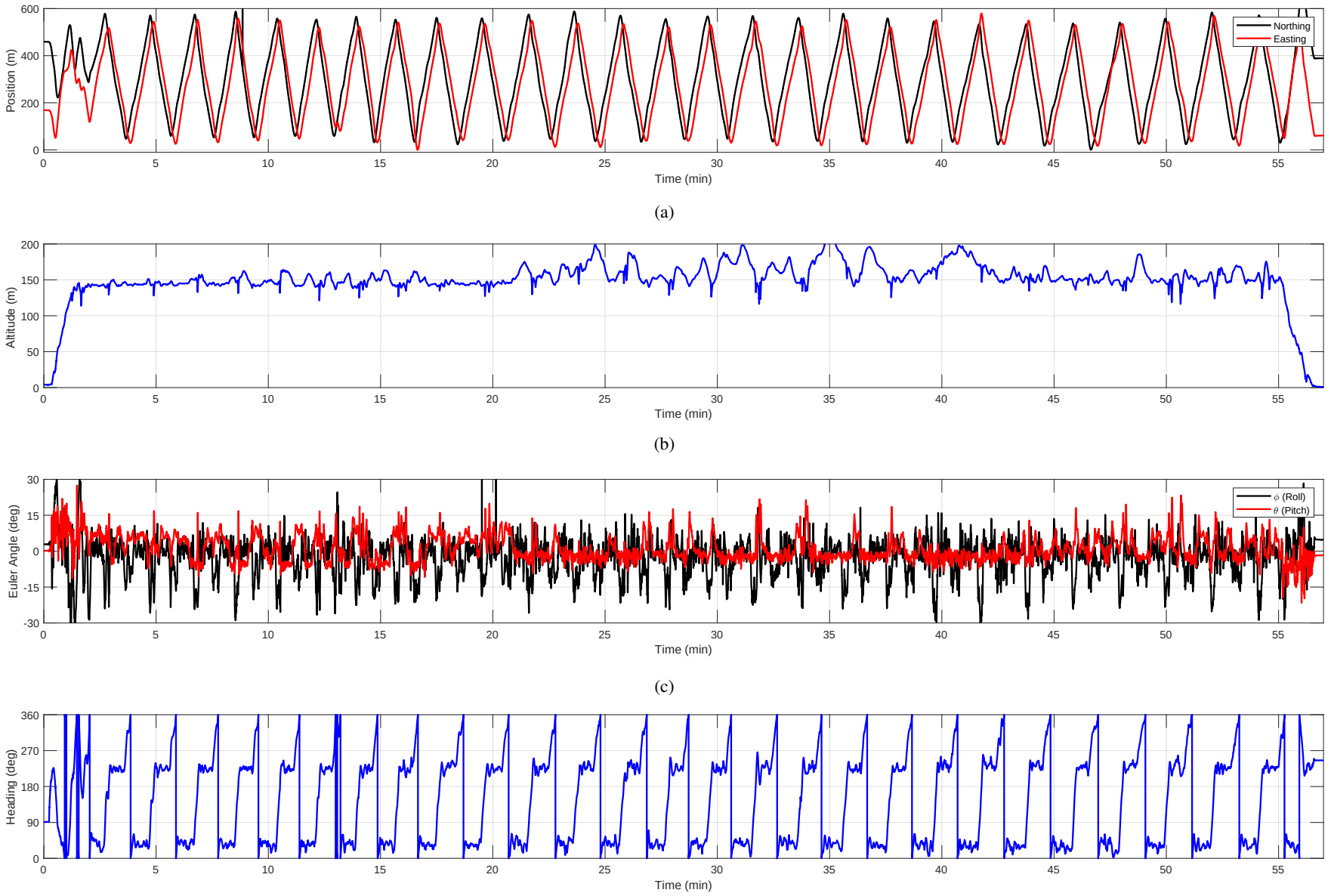

Figure 7: The state data time history of the UIUC-TUM Solar Flyer performing the approximately 1 hour flight under ideal conditions: (a) Northing and Easting position, (b) altitude, (c) pitch and roll, (d) heading.

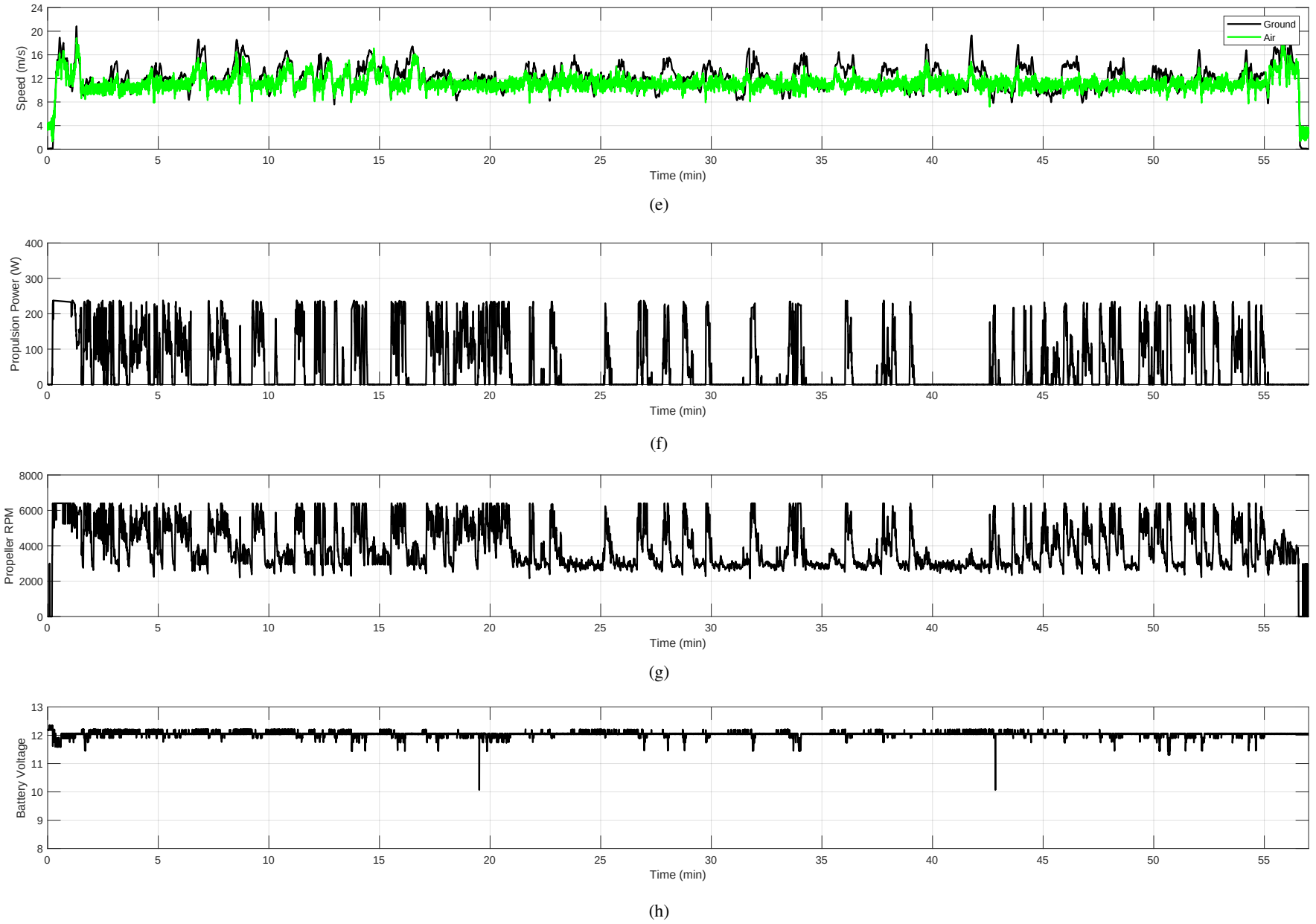

Figure 5 (continued): The state data time history of the UIUC-TUM Solar Flyer performing the approximately 1 hour flight under ideal conditions: (e) air and ground speed, (f) propulsion power consumption, (g) propeller rotation rate in RPM, (h) battery voltage.

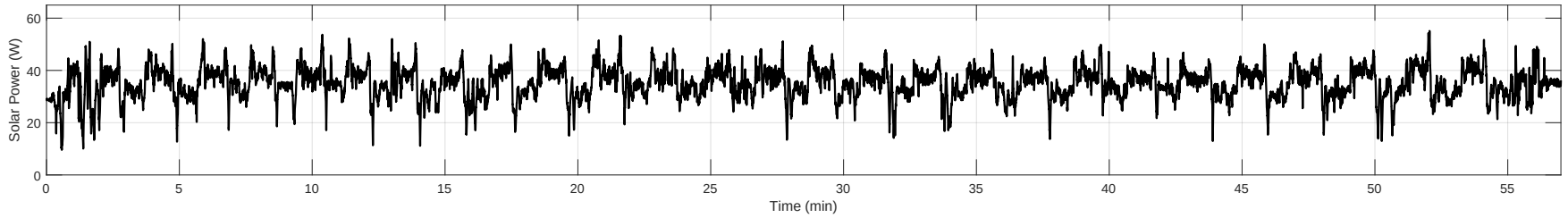

(i)

Figure 5 (continued): The state data time history of the UIUC-TUM Solar Flyer performing the approximately 1 hour flight under ideal conditions: (i) solar power generated.

IV. Integrated Power Simulation

Long-duration flight simulation for the UIUC-Solar Flyer was performed using the integrated power model. First, the simulation setup and aircraft parameters used are discussed. Then, in an attempt to duplicate the flight results of the Oct 1, 2020 flight test, a 26-lap flight simulation is performed; the results of this simulation are compared to the flight test results.

A. Simulation Setup and Aircraft Parameters

Flight simulation using the integrated power model was implemented in Matlab. The resulting code-base consists of: (1) a setup script which defines the initial conditions and aircraft parameters (described below), (2) a trajectory and state estimator that translates a pre-defined set of flight instructions, consisting of distances, velocities, climb/descent angles, and turn radii, into temporal and spatial aircraft state data; and (3) energy state estimator, which uses the aforementioned aircraft parameters and state data to estimate aircraft propulsion power consumption, solar power generation, and onboard energy levels. The energy state estimator also determines intermediate propulsion system state data, including propeller rotation rate and component efficiencies.

Aircraft parameters for the UIUC-TUM Solar Flyer were determined through physical measurement of the aircraft, estimation based on past flight testing results, and component specification. The parameters used in the following long-duration simulations are summarized below in Table 1. The propeller performance data for the Aero-Naut CAM 12x8 folding propeller used on the UIUC-TUM Solar Flyer is presented in Fig. 8. The battery cell discharge curves for the Samsung 35E 18650 li-ion cells used on the aircraft are presented in Fig. 9 and are based on external testing results.[65]

B. 1 Hour Flight Simulation

Flight simulation was performed to duplicate the experimental results of the 26-lap, approximately-hour-long flight on Oct 8, 2020 flight test. As per the actual flight, the start time of the simulation was defined as 11:43 AM Oct 8, 2020, which also defined the corresponding sun location. The atmospheric density was set to 1.19 kg/m^3, and the solar flux values were input from measurements taken at a local weather station. Wind was not simulated. Per the actual flight test, the aircraft trajectory was set to 26 laps of an identically-oriented race track pattern of 650×150 m at an altitude of 150 m AGL and speed of 11 m/s.

The trajectory of the flight is shown in Fig. 10 with the same perspective as used in the experimental 1-hour flight. Unlike the experimental flight, the simulated flight performed only the race track laps, without the takeoff, ascent, descent, and landing. The simulated state data time history is presented in Fig. 11, with similar data being presented in (a)-(i). The vertical axes limits and ticks of each plot are identical to those presented for the experimental data in Fig. 7. Meanwhile, each plot's horizontal axis limits and ticks are only slightly longer than those presented for the experimental data (60 min vs. 57 min).

Table 1: Simulation parameters used to model the UIUC-TUM Solar Flyer aircraft.

Aircraft Physical Parameters	
Mass (m)	3.3 kg (7.2 lb)
Wing Area (S)	85 dm^2 (1318 in^2)
Aspect Ratio (AR)	18.8
Aircraft Performance Properties	
Oswald Efficiency Factor (e)	0.95
Zero-Lift Drag Coefficient (C_{D_o})	0.01956
Propulsion Properties	
Propeller Performance and Efficiency Curves	See Fig. 8
Motor Speed Constant (K_v)	840 RPM/V
Motor Internal Resistance (R_m)	0.145 Ω
Motor Zero Load Current (i_0)	0.70 A
Motor Maximum Power	425 W
ESC Efficiency (η_{ESC})	85 %
Battery Properties	
Total Number of Cells	24
Series Number of Cells	3
Parallel Number of Cells	8
Maximum Battery Voltage	4.2 V
Minimum Battery Voltage	3.0 V
Battery Cell Energy Capacity	∼12.0 W-H
Battery Cell Discharge Curves	See Fig. 9
Battery Charge Efficiency	90 %
Battery Discharge Efficiency	90 %
Solar Properties	
Solar Conversion Efficiency (η_{solar})	25 %
Solar 5-Cell Array Area ($A_{area_{5cell}}$)	0.004275 m^2
Total Number of 5-Cell Solar Arrays	64
Number of 5-Cell Solar Arrays per Wing Panel Sub-Array (L-R)	11, 13, 8, 8, 13, 11
Wing Panel Sub-Array (L-R) Roll Angle	12.0, 7.0, 2.0, -2.0, -7.0, -12.0 deg
Solar Array Average Pitch Angle	2.6 deg
Solar Angular Performance (η_{array})	Lambert's Cosine Law
MPPT Efficiency (η_{MPPT})	88 %

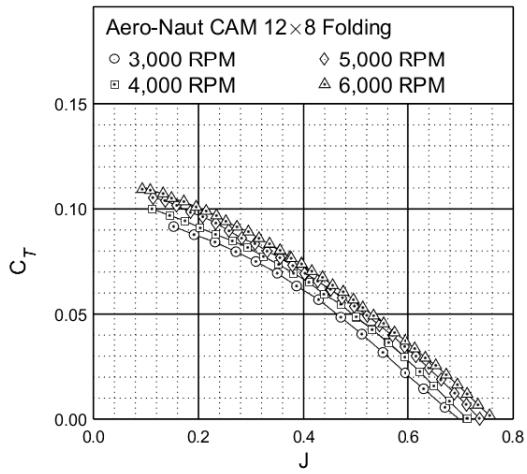

(a)

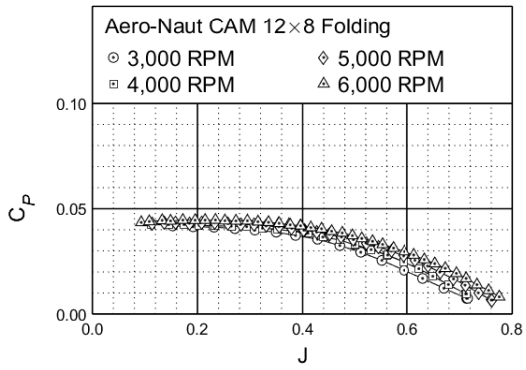

(b)

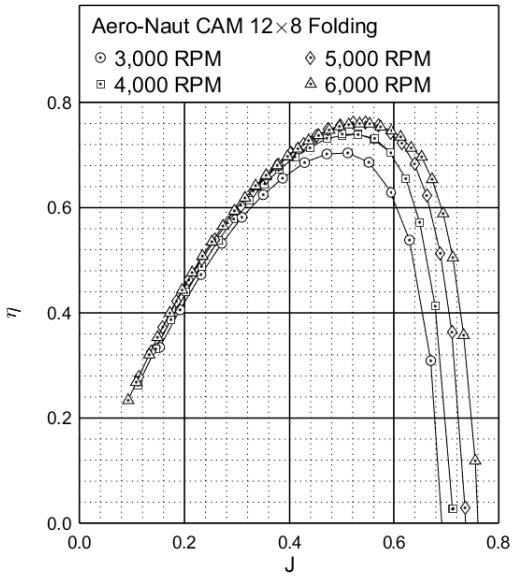

(c)

Figure 8: Propeller performance curves for the Aeronaut CAM 12x8 propeller used on the UIUC-TUM Solar Flyer from 2020 and forward: (a) thrust (C_T), (b) power (C_P), and (c) efficiency $(\eta_{propeller})$ vs. advance ratio (J)

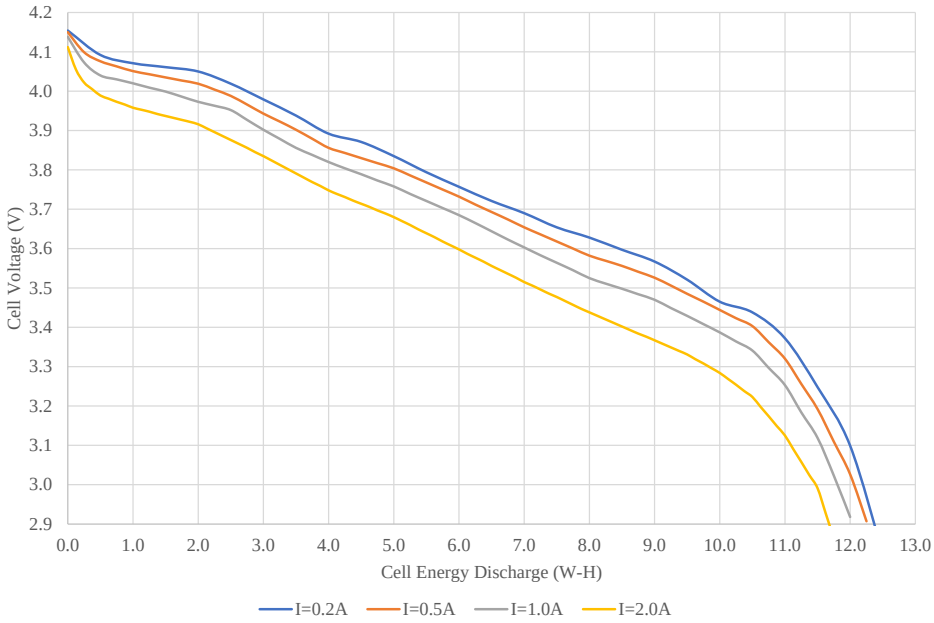

Figure 9: Battery cell discharge curves for the Samsung 35E 18650 li-ion cells under varying discharge currents (based on external testing[65]).

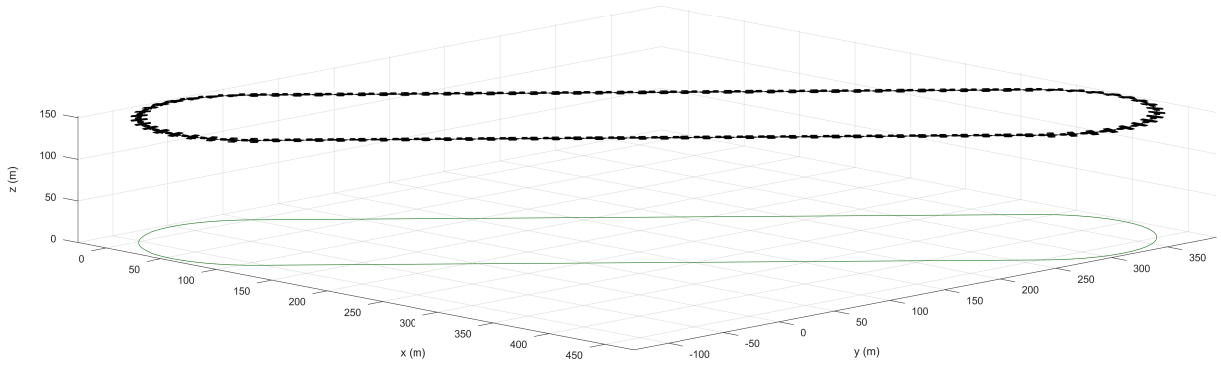

Figure 10: The simulated trajectory of the UIUC-TUM Solar Flyer, attempting to duplicate the flight test performed on Oct 8, 2020 (note that the aircraft is plotted every 5 sec).

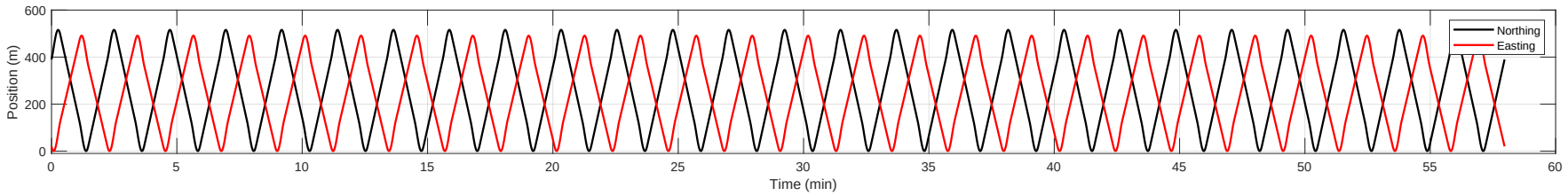

(a)

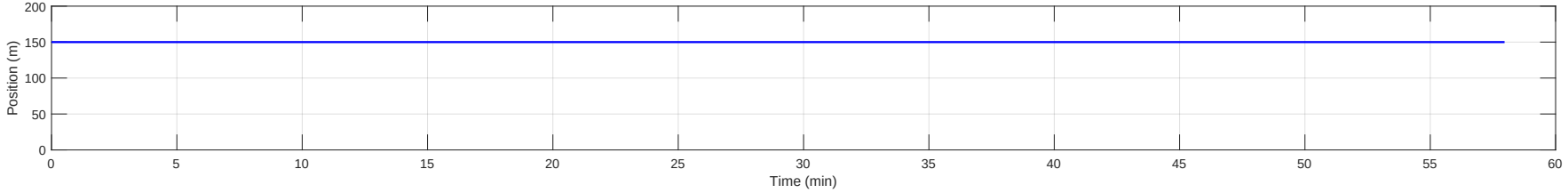

(b)

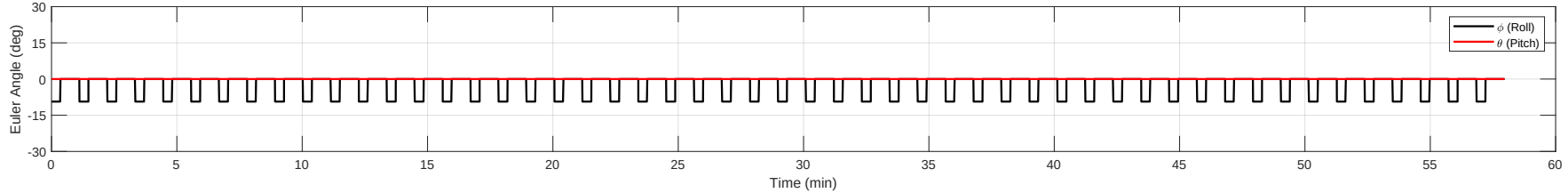

(c)

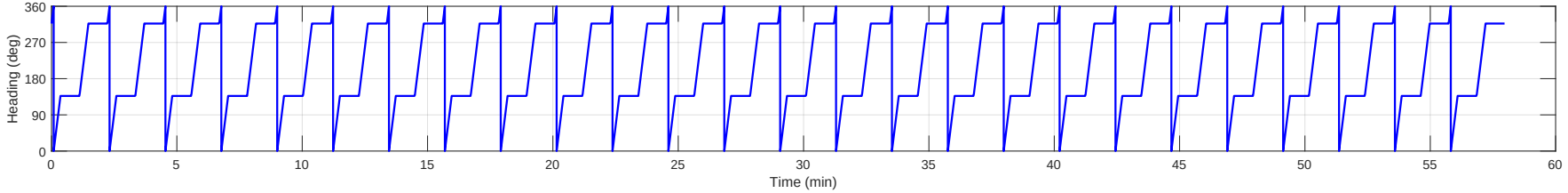

(d)

Figure 11: The simulated state data time history of the UIUC-TUM Solar Flyer, attempting to duplicate the flight test performed on Oct 8, 2020: (a) Northing and Easting position, (b) altitude, (c) pitch and roll, (d) heading.

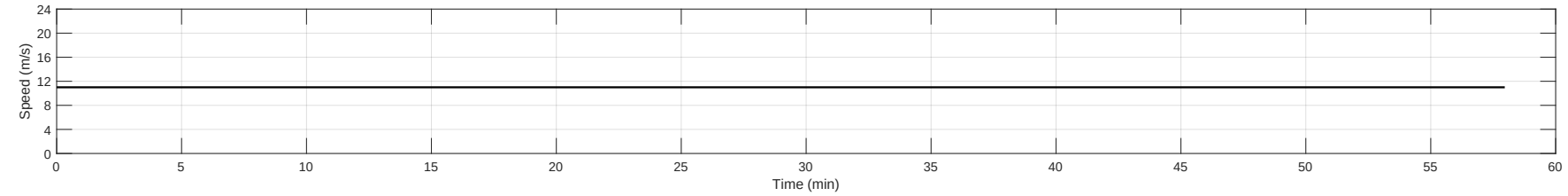

(e)

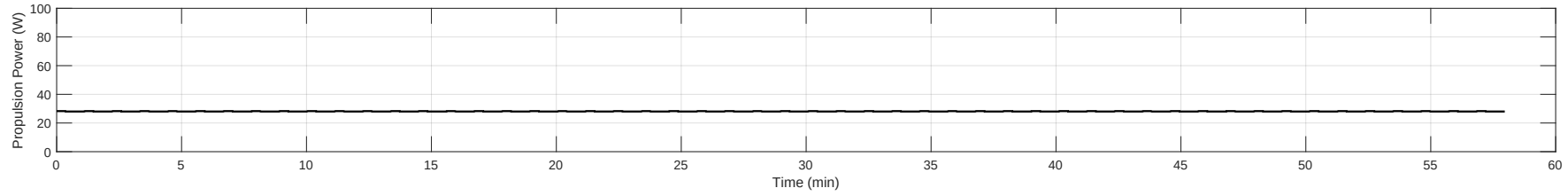

(f)

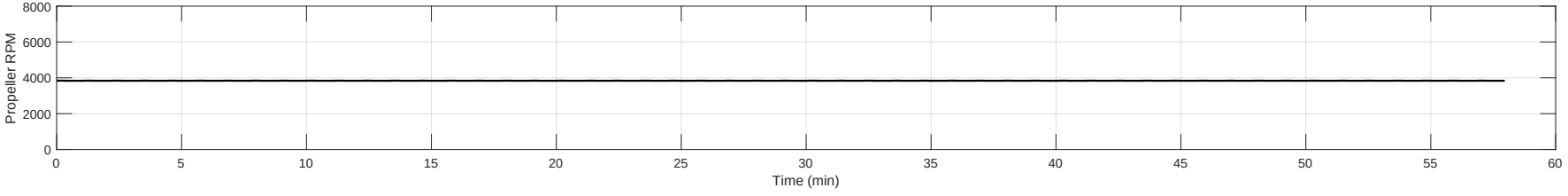

(g)

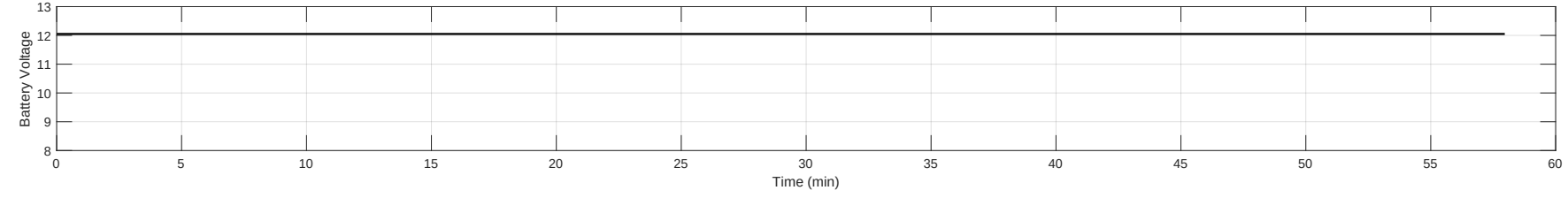

(h)

Figure 5 (continued): The simulated state data time history of the UIUC-TUM Solar Flyer, attempting to duplicate the flight test performed on Oct 8, 2020: (e) air and ground speed, (f) propulsion power consumption, (g) propeller rotation rate in RPM, (h) battery voltage.

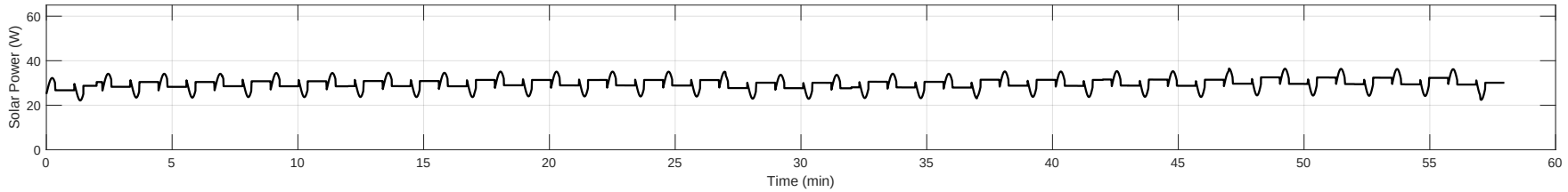

(i)

Figure 5 (continued): The simulated state data time history of the UIUC-TUM Solar Flyer, attempting to duplicate the flight test performed on Oct 8, 2020: (i) solar power generated.

C. Comparison of Simulated and Experimental Flight Test Results

Comparing the simulated and experimental flight test trajectories shows the difference between an ideal flight path and one influenced by external factors. Specifically, since simulation has no environmental factors, i.e., horizontal winds or vertical air draft, the race track trajectory is perfectly repeated between laps. Meanwhile, the experimental trajectory shows significant horizontal differences between each lap and vertical excursions previously mentioned. The difference can be further examined by observing the position state data in (a) and (b) of the respective figures. As is expected, the simulated state data shows perfectly repeated Northing and Easting position oscillations while the experimental state data varies. For altitude, the simulated data is constant at 150 m while the experimental data varies by as much as 50 m, likely due to thermals and vertical air drafts.

Examining the Euler angle state data in (c) and (d) in the respective figures once again shows ideal patterns in simulated flight data and noisy patterns with large overshoots in experimental flight data. Specifically, in the simulated data, pitch is maintained near zero for the entire flight. The aircraft is instantaneously rolled to -10 deg in turns, with the heading changing linearly during those corresponding turns; previous work has quantified the deviations expected by simulating turns with instantaneous roll changes.[66] Meanwhile, the experimental data shows very noisy, non-zero data for pitch with values oscillating between -10 and 15 deg, often corresponding to altitude excursions but also to recovery from turns. The experimental roll data is also quite noisy, with values mostly oscillating between -20 and 10 deg, mainly during turns; the aircraft is often seen to overshoot the desired 10 deg bank angle and overshoot level recovery. Finally, the experimental heading data is similar to the simulated patterns with constant oscillations seen throughout the data.

Similar to the previous comparisons, in (e), aircraft speed in simulation is constantly 11 m/s, while the experimental data oscillates about that value due to altitude variations, among other factors. The difference is easily explained in how the aircraft speed is regulated per se. In simulation, the velocity is prescribed, while in experimental flight testing, the autopilot controller attempts to maintain a desired airspeed with the aircraft experiencing varied environmental conditions and orientations. Hence, the propulsion power and propeller rotation rate differences are similar in respective (f) and (g). In simulation, the propulsion power and propeller rotation rate instantaneously change as required to meet the aircraft thrust requirement resulting from the prescribed aircraft velocity and orientation. This yields constant propulsion power in level flight with very slight increases of 1.5 % in turns. Overall, the average simulated propulsion power consumption is 28.1 W. As mentioned earlier, in experimental flight testing, there is an interplay between the autopilot velocity controller and the ESC controller with significant environmental factors at play, which causes repeated throttling-on and throttling-off of the motor. This creates the corresponding spikes of propulsion power and propeller rotation rate. Thus, the experimentally measured propulsion power highly varies throughout the flight due to environmental difference, with 10 min (5 laps of 60,000 data points each) averages for propulsion power consumption ranging from 14 and 53 W. The average simulated propulsion power consumption of 28.1 W lies nicely within the experimental 10 min average range of 14 and 53 W.

Comparison of the simulated and experimental solar power generation in (i) shows similar flight path-dependent trends with precise repeated curves occurring for the simulated results and very noisy data occurring for the experimental results. Both results show an obvious correlation to the aircraft's flight path with constant trends occurring for level flight; there are slightly higher values in one direction than the other for both results. During the turns, the power generation either increases or decreases due to the aircraft's orientation relative to the sun. The simulated data has ideal repeated data as it is orientation is exactly followed. Meanwhile, with the large number of overshoots and oscillatory aircraft orientation, the experimental data shows a high level of oscillations about the trend. The average simulated solar power generation is 29.7 W, which is similar to the average experimental solar power generation is approximately 35 W. The difference in average solar power generation values may possibly be differences in aircraft in-flight wing and thus solar array orientations, the value of solar array conversion efficiency, and the actual solar flux encountered compared to

that measured at a nearby weather station. Finally, as propulsion power consumption is well balanced with solar power generation, the battery voltage in (h) is expectedly constant for both the simulated and experimental flight test results,

V. Summary and Future Work

This paper presented and compared simulation results for a long-endurance, solar-powered unmanned aircraft using an integrated aircraft power model for solar generation and aircraft propulsion. The power consumption and generation models were described, derived, and integrated into a cohesive system-wide aircraft power model presented in the form of a systemic flow diagram. Power balance expressions were imposed based on temporal and physical constraints. The UIUC-TUM Solar Flyer, a computationally-intensive, long-endurance solar-powered unmanned aircraft of interest was used as an example aircraft for the simulation. A simulation was presented that attempted to duplicate a recent long-endurance flight the Solar Flyer experimentally performed in under ideal conditions. The simulated and experimental flight test results were compared, showing high similarity.

For future work, longer-duration simulations with complex mission trajectories are planned. The integrated power model and simulation should be enhanced to simulate temporal environmental conditions such as horizontal wind, vertical air drafts (e.g., thermals), and turbulence. Additional flight testing for further comparison and refinement of modeling and simulation is also desired. These improvements will allow for greater fidelity power modeling and simulation that could be applied to various application scenarios.

Acknowledgments

The material presented in this paper is based upon work supported by the National Science Foundation (NSF) under grant number CNS-1646383 and by the Center for Digital Agriculture (CDA) at the University of Illinois at Urbana-Champaign under a seed funding award. Marco Caccamo was also supported by an Alexander von Humboldt Professorship endowed by the German Federal Ministry of Education and Research. Any opinions, findings, and conclusions or recommendations expressed in this publication are those of the authors and do not necessarily reflect the views of the NSF or CDA.

References

[1]Precision Hawk, "Precision Agriculture, Commercial UAV and Farm Drones," `http://precisionhawk.com/`, Accessed Apr. 2015.

[2]MicroPilot, "MicroPilot - MP-Vision," `http://www.micropilot.com/products-mp-visione.htm`, Accessed May. 2015.

[3]AeroVironment Inc., "Quantix," `https://www.avdroneanalytics.com/quantix/`, Accessed Dec. 2019.

[4]Pix4D SA, "Pix4D," `https://www.pix4d.com/`, Accessed Dec. 2019.

[5]Reconstruct Inc., "Reconstruct," `https://www.reconstructinc.com/`, Accessed Dec. 2019.

[6]Real Time and Embedded System Laboratory, University of Illinois at Urbana-Champaign, "Solar-Powered Long-Endurance UAV for Real-Time Onboard Data Processing," `http://rtsl-edge.cs.illinois.edu/UAV/`, Accessed Jan. 2021.

[7]Green, C. R. and McDonald, R. A., "Modeling and Test of the Efficiency of Electronic Speed Controllers for Brushless DC Motors," AIAA Paper 2015-3191, AIAA Aviation Forum, Dallas, TX, Jun. 2015.

[8]McCrink, M. H. and Gregory, J. W., "Blade Element Momentum Modeling for Low-Re Small UAS Electric Propulsion Systems," AIAA Paper 2015-3191, AIAA Aviation Forum, Dallas, TX, Jun. 2015.

[9]Lundstrom, D., Amadori, K., and Krus, P., "Validation of Models for Small Scale Electric Propulsion Systems," AIAA Paper 2010-483, AIAA Aerospace Sciences Meeting, Orlando, FL, Jan. 2010.

[10]Ostler, J. and Bowman, W., "Flight Testing of Small, Electric Powered Unmanned Aerial Vehicles," U.S. Air Force T&E Days Conferences, American Institute of Aeronautics and Astronautics, Dec. 2005.

[11]Lee, J. S. and Yu, K. H., "Optimal Path Planning of Solar-Powered UAV Using Gravitational Potential Energy," *IEEE Transactions on Aerospace and Electronic Systems*, Vol. 53, No. 3, Jun. 2017, pp. 1442–1451.

[12]Grano-Romero, C., García-Juárez, M., Guerrero-Castellanos, J. F., Guerrero-Sánchez, W. F., Ambrosio-Lázaro, R. C., and Mino-Aguilar, G., "Modeling and control of a fixed-wing UAV powered by solar energy: An electric array reconfiguration approach," *2016 13th International Conference on Power Electronics (CIEP)*, Jun. 2016, pp. 52–57.

[13]Gao, X.-Z., Hou, Z.-X., Guo, Z., Liu, J.-X., and Chen, X.-Q., "Energy management strategy for solar-powered high-altitude long-endurance aircraft," *Energy Conversion and Management*, Vol. 70, No. Supplement C, 2013, pp. 20 – 30.

[14]Hosseini, S., Dai, R., and Mesbahi, M., "Optimal path planning and power allocation for a long endurance solar-powered UAV," *2013 American Control Conference*, Jun. 2013, pp. 2588–2593.

[15]B. Lee, B., Park, P., Kim, C., Yang, S., and Ahn, S., "Power managements of a hybrid electric propulsion system for UAVs," *Journal of Mechanical Science and Technology*, Vol. 26, No. 8, Aug 2012, pp. 2291–2299.

[16]Gong, A., MacNeill, R., and Verstraete, D., "Performance Testing and Modeling of a Brushless DC Motor, Electronic Speed Controller and Propeller for a Small UAV," AIAA Paper 2018-4584, AIAA Propulsion and Energy Forum, Cincinnati, OH, Jul. 2018.

[17]Gong, A. and Verstraete, D., "Experimental Testing of Electronic Speed Controllers for UAVs," AIAA Paper 2017-4955, AIAA/SAE/ASEE Joint Propulsion Conference, Atlanta, GA, Jul. 2017.

[18]Gong, A., Maunder, H., and Verstraete, D., "Development of an in-fight thrust measurement system for UAVs," AIAA Paper 2017-5092, AIAA/SAE/ASEE Joint Propulsion Conference, Atlanta, GA, Jul. 2017.

[19]Karabetsky, D., "Solar rechargeable airplane: Power system optimization," *2016 4th International Conference on Methods and Systems of Navigation and Motion Control (MSNMC)*, Oct. 2016, pp. 218–220.

[20]Park, H. B., Lee, J. S., and Yu, K. H., "Flight evaluation of solar powered unmanned flying vehicle using ground testbed," *2015 15th International Conference on Control, Automation and Systems (ICCAS)*, Oct. 2015, pp. 871–874.

[21]Lindahl, P., Moog, E., and Shaw, S. R., "Simulation, Design, and Validation of an UAV SOFC Propulsion System," *IEEE Transactions on Aerospace and Electronic Systems*, Vol. 48, No. 3, Jul. 2012, pp. 2582–2593.

[22]Brandt, J. B. and Selig, M. S., "Propeller Performance Data at Low Reynolds Numbers," AIAA Paper 2011-1255, AIAA Aerospace Sciences Meeting, Orlando, FL, Jan. 2011.

[23]Shiau, J. K., Ma, D. M., Chiu, C. W., and Shie, J. R., "Optimal Sizing and Cruise Speed Determination for a Solar-Powered Airplane," *AIAA Journal of Aircraft*, Vol. 47, No. 2, Mar. 2010, pp. 622–629.

[24]Khan, W. and Nahon, M., "Modeling dynamics of agile fixed-wing UAVs for real-time applications," *2016 International Conference on Unmanned Aircraft Systems (ICUAS)*, Jun. 2016, pp. 1303–1312.

[25]Selig, M. S., "Real-Time Flight Simulation of Highly Maneuverable Unmanned Aerial Vehicles," *Journal of Aircraft*, Vol. 51, No. 6, Nov.-Dec. 2014, pp. 1705–1725.

[26]Johnson, E. N. and Mishra, S., "Flight Simulation for the Development of an Experimental UAV," AIAA Paper 2002-4975, AIAA Modeling and Simulation Technologies Conference and Exhibit, Monterey, CA, Aug. 2002.

[27]FlightGear Flight Simulator, "FlightGear," http://www.flightgear.org, Accessed Oct. 2017.

[28]Dantsker, O. D., Theile, M., and Caccamo, M., "Integrated Power Modeling for a Solar-Powered, Computationally-Intensive Unmanned Aircraft," AIAA Paper 2020-3568, 2020 AIAA/IEEE Electric Aircraft Technologies Symposium, Virtual Forum, Aug. 2020.

[29]Rayleigh, L., "The Soaring of Birds," *Nature*, Vol. 27, Apr. 1883, pp. 534–535.

[30]Hendriks, F., *Dynamic Soaring*, Ph.D. thesis, Univ. of CA, Los Angles, CA, 1972.

[31]Barnes, J. P., "How Flies the Albatross—The Flight Mechanics of Dynamic Soaring," *SAE Paper 2004-01-3088, Nov. 2004*.

[32]Sukumar, P. P. and Selig, M. S., "Dynamic Soaring of Sailplanes over Open Fields," *Journal of Aircraft*, Vol. 50, No. 5, Sep.-Oct. 2013, pp. 1420–1430.

[33]Woodbury, T., Dunn, C., and Valasek, J., "Autonomous Soaring Using Reinforcement Learning for Trajectory Generation," AIAA Paper 2014-0990, AIAA SciTech Forum, National Harbor, MD, Jan. 2014.

[34]Bird, J. J. and Langelaan, J. W., "Optimal Speed Scheduling for Hybrid Solar Aircraft with Arrival Time Condition," AIAA Paper 2019-1421, AIAA SciTech Forum, San Diego, CA, Jan. 2019.

[35]Shiau, J. K., Ma, D. M., Yang, P. Y., Wang, G. F., and Gong, J. H., "Design of a Solar Power Management System for an Experimental UAV," *IEEE Transactions on Aerospace and Electronic Systems*, Vol. 45, No. 4, Oct. 2009, pp. 1350–1360.

[36]Iqbal, M., "An Introduction to Solar Radiation," 1983.

[37]Michalsky, J. J., "The Astronomical Almanac's algorithm for approximate solar position (1950–2050)," *Solar Energy*, Vol. 40.

[38]Meeus, J., *Astronomical Algorithms, 2nd Edition*, Willmann-Bell, Inc., Richmond, VA, 1999.

[39]Kumar, L., Skidmore, A. K., and Knowles, E., "Modelling topographic variation in solar radiation in a GIS environment," *International Journal of Geographical Information Science*, Vol. 11, No. 5, 1997, pp. 475–497.

[40]Jenkins, A., "The Sun's position in the sky," *European Journal of Physics*, Vol. 34, No. 3, Mar. 2013, pp. 633–652.

[41]Reda, I. and Andreas, A., "Solar Position Algorithm for Solar Radiation Applications," Tech. rep., US Department of Energy, National Renewable Energy Laboratory, NREL/TP-560-34302, 2008.

[42]Walker, C. and Vaucher, G., "Atmospheric Renewable Energy Research,Volume 5 (Solar Radiation Flux Model)," Tech. rep., US Army Research Laboratory, ARL-TR-8155, 2017.

[43]Khatib, T. and Elmenreich, W., *Modeling of Photovoltaic Systems Using MATLAB: Simplified Green Codes*, John Wiley & Sons, Inc., Hoboken, NJ, 2016.

[44]Hebeler, F., "Solar Radiation," `https://www.mathworks.com/matlabcentral/fileexchange/19791-solar-radiation`, 2020.

[45]McCormick, B. W., *Aerodynamics, Aeronautics, and Flight Mechanics, 2nd Edition*, John Wiley & Sons, Inc., Hoboken, NJ, 1994.

[46]Dantsker, O. D., Theile, M., and Caccamo, M., "A High-Fidelity, Low-Order Propulsion Power Model for Fixed-Wing Electric Unmanned Aircraft," AIAA Paper 2018-5009, AIAA/IEEE Electric Aircraft Technologies Symposium, Cincinnati, OH, Jul. 2018.

[47]Ol, M., Zeune, C., and Logan, M., "Analytical/Experimental Comparison for Small Electric Unmanned Air Vehicle Propellers," *26th AIAA Applied Aerodynamics Conference*, American Institute of Aeronautics and Astronautics, Reston, VA, 8 2008.

[48]Dantsker, O. D., Caccamo, M., Deters, R. W., and Selig, M. S., "Performance Testing of Aero-Naut CAM Folding Propellers," AIAA Paper 2020-2762, AIAA Aviation Forum, Virtual Event, Jun. 2020.

[49]UIUC Applied Aerodynamics Group, "UIUC Propeller Data Site," `http://m-selig.ae.illinois.edu/props/propDB.html`.

[50]O. Dantsker and R. Mancuso and M. Vahora, "Unmanned Aerial Vehicle Database," `http://uavdb.org/`.

[51]Dantsker, O. D., Imtiaz, S., and Caccamo, M., "Electric Propulsion System Optimization for a Long-Endurance and Solar-Powered Unmanned Aircraft," AIAA Paper 2019-4486, AIAA/IEEE Electric Aircraft Technology Symposium, Indianapolis, Indiana, Aug. 2019.

[52]Drela, M., "First-Order DC Electric Motor Model," http://web.mit.edu/drela/Public/web/qprop/motor1_theory.pdf, Accessed May 2020.

[53]Drela, M., "Second-Order DC Electric Motor Model," http://web.mit.edu/drela/Public/web/qprop/motor2_theory.pdf, Accessed May 2020.

[54]Dantsker, O. D., Theile, M., Caccamo, M., and Mancuso, R., "Design, Development, and Initial Testing of a Computationally-Intensive, Long-Endurance Solar-Powered Unmanned Aircraft," AIAA Paper 2018-4217, AIAA Applied Aerodynamics Conference, Atlanta, GA, Jun. 2018.

[55]Dantsker, O. D., Theile, M., Caccamo, M., Yu, S., Vahora, M., and Mancuso, R., "Continued Development and Flight Testing of a Long-Endurance Solar-Powered Unmanned Aircraft: UIUC-TUM Solar Flyer," AIAA Paper 2020-0781, AIAA Scitech Forum, Orlando, FL, Jan. 2020.

[56]Dantsker, O. D., Imtiaz, S., and Caccamo, M., "Propulsion System Design, Optimization, Simulation, and Testing for a Long-Endurance Solar-Powered Unmanned Aircraft," AIAA Propulsion and Energy Forum, Virtual Event, Aug. 2020.

[57]Al Volo LLC, "Al Volo: Flight Systems," http://www.alvolo.us, Accessed Jun. 2019.

[58]Dantsker, O. D. and Mancuso, R., "Flight Data Acquisition Platform Development, Integration, and Operation on Small- to Medium-Sized Unmanned Aircraft," AIAA Paper 2019-1262, AIAA SciTech Forum, San Diego, California, Jan 2019.

[59]Mirco Theile, "uavAP: A Modular Autopilot for Unmanned Aerial Vehicles," https://github.com/theilem/uavAP.

[60]Theile, M., Dantsker, O. D., Caccamo, M., and Yu, S., "uavAP: A Modular Autopilot Framework for UAVs," AIAA Paper 2020-3268, AIAA Aviation Forum, Virtual Event, Jun. 2020.

[61]Mirco Theile, "uavGS: A Modular Ground Control Station Interface for Unmanned Aerial Vehicles," https://github.com/theilem/uavGS.

[62]Theile, M., Dantsker, O. D., Nai, R., and Caccamo, M., "uavEE: A Modular, Power-Aware Emulation Environment for Rapid Prototyping and Testing of UAVs," IEEE International Conference on Embedded and Real-Time Computing Systems and Applications, Hakodate, Japan, Aug. 2018.

[63]Dantsker, O. D., Theile, M., and Caccamo, M., "A Cyber-Physical Prototyping and Testing Framework to Enable the Rapid Development of UAVs," *Submitted to Aerospace*, 2021.

[64]Dantsker, O. D., Theile, M., and Caccamo, M., "Long Endurance Flight Testing Results for the UIUC-TUM Solar Flyer," AIAA Paper 2021-3196, AIAA Aviation Forum, Virtual Event, Aug. 2021.

[65]"Samsung INR18650-35E 3500mAh (Pink)," https://lygte-info.dk/review/batteries2012/SamsungINR18650-35E3500mAh(Pink)UK.html.

[66]Theile, M., Yu, S., Dantsker, O. D., and Caccamo, M., "Trajectory Estimation for Geo-Fencing Applications on Small-Size Fixed-Wing UAVs," IEEE International Conference on Intelligent Robots and Systems, Macau, China, Nov. 2019.